JOURNAL OF GEOPHYSICAL RESEARCH, VOL. 106, NO. D15, PAGES 17,133–17,146, AUGUST 16, 2001

Relationship between upper tropospheric humidity and deep convection

Fabrizio Sassi
Atmospheric Systems and Analysis, Westminster, Colorado

Murry Salby
University of Colorado, Boulder, Colorado

William G. Read
Jet Propulsion Laboratory, California Institute of Technology, Pasadena, California

Abstract. Satellite measurements of upper tropospheric humidity (UTH) are used together with global cloud imagery to study the relationship between deep convection and moisture in the upper troposphere. Throughout the tropics, regions of cold cloud coincide with regions of enhanced UTH,in time-mean distributions, in daily synoptic maps, and even on the short scales that characterize individual convective systems. Cold-cloud fraction and UTH have very similar instantaneous structure. The horizontal correlation scales are narrow for both cloud fraction and UTH at 315 hPa and 215 hPa. The correlation scale of UTH expands at 146 hPa, signaling an increased role of horizontal transport. Ventilation of the upper troposphere by convection is also evidenced by thermal structure: Inside regions of deep convection the vertical separation of θ surfaces is expanded, stability being weakened by convective mixing inside a deep layer centered near 200 hPa. Supported by a cloud detrainment, convection humidifies the upper troposphere, elevating mixing ratio surfaces over their surroundings. The reverse is observed at subtropical latitudes, where air is anomalously dry. Jointly, these features characterize vertical transport by the Hadley and Walker circulations.

1. Introduction

Water vapor is the most important trace constituent of the atmosphere. Because of its strong absorption of longwave radiation, the distribution and variability of water vapor figure centrally in considerations of climate. Many of the issues involving water vapor concern its feedback with temperature, the understanding of which is limited by uncertainties surrounding the distribution of humidity in the upper troposphere.

Column abundance of water maximizes in the tropics, where vertical transport is concentrated inside convective towers [*Riehl and Malkus,* 1958]. Understanding upper tropospheric humidity (UTH) therefore requires an understanding of how it is related to deep convection that invades the upper troposphere.

Establishing such a relationship requires accurate measurements of humidity at upper levels, where mixing ratios have decreased to only a few hundred parts per million. UTH is poorly measured in conventional observations, because of the limited sensitivity and sparse coverage of radiosondes and because of the coarse vertical resolution of satellite measurements. In addition, IR measurements made by satellites are limited to clear-sky regions. Microwave measurements from nadir-viewing satellites measure UTH in cloudy regions, but again with coarse vertical resolution.

In this study, we employ microwave observations of UTH made by the Microwave Limb Sounder (MLS) on board the Upper Atmospheric Research Satellite (UARS) [*Waters et al.*, 1999]. The limb-viewing microwave technique is distinguished from conventional measurements of water vapor by its observation of UTH in cloudy as well as in clear-sky regions [*Read et al.*, 1995]. It also observes water vapor over continental regions as well as over maritime regions. MLS observations therefore provide a uniform description of upper tropospheric humidity. UTH observations are complemented by observations of cold cloud in high-resolution global cloud imagery (GCI), which has been composited from six satellites simultaneously observing the Earth [*Salby et al.*, 1991]. Available globally every 3 hours, the GCI provides a continuous record of convection, against which coincident UTH measurements from MLS can be compared.

Paper number 2001JD900121.
0148-0227/2001/2001JD900121$09.00

Following a description of the data and analysis, Section 3 discusses the three-dimensional distributions of humidity and convection. Section 4 then develops the instantaneous structure of UTH, which is shown to behave very similarly to that of cold-cloud fraction. Section 5 examines the signature of convection in thermal structure, which likewise shares features with the distribution of UTH. These features are shown to mark regions of local upwelling and downwelling, which comprise the Hadley and Walker circulations. Section 6 then develops a statistical description of UTH that quantifies its forcing, locally inside regions of convection and globally over the tropics as a whole, and then evaluates its sensitivity to changes of deep convection.

2. Data and Analysis

MLS observes upper tropospheric relative humidity asynoptically through radiances measured in its 205 GHz channel [*Read et al.*, 1995]. Data used in this study are taken from the Version 4.9 retrieval, which provides UTH at four pressure levels approximately 2.7 km apart: 464, 315, 215, and 146 hPa. Accuracy of MLS UTH depends on the amount of water vapor present, measurements being more accurate at about 215 hPa. More specifically, the nominal accuracy of individual UTH measurements between 30°S and 30°N is 34% relative humidity with respect to ice (RHi) at 147 hPa, 20% RHi at 215 hPa, and 20% RHi at 316 hPa. These levels represent UTH at levels where conventional measurements are inaccurate and with much finer vertical resolution than is available from other satellite measurements.

In addition to asynoptic retrievals of UTH we also make use of time-mean and daily synoptic distributions. Retrieved values of UTH have been synoptically mapped via an algorithm that rejects undersampled convective structure [*Salby and Sassi*, 2000], enabling daily distributions of UTH to be mapped on those space and timescales resolved in the asynoptic data. Describing large-scale coherent variations of UTH, such distributions have been produced for the nominal observing period of MLS, between October 1991 and September 1994.

Complementing MLS observations of UTH is high-resolution Global Cloud Imagery. The GCI is composited from four geostationary (GMS, GEOS-E, GEOS-W, METEOSAT) and two polar-orbiting (NOAA 7 and NOAA 8) platforms that simultaneously observe the Earth [*Tanaka et al.*, 1991]. It is comprised of synoptic global images of 11-μm brightness temperature, every 3 hours, each with 0.5° horizontal resolution. The GCI captures the major space and timescales of organized convection, including mesoscale convective systems and several harmonics of the diurnal cycle. Its high spatial and temporal resolution, global coverage, and continuity provide observations of cloud where and when MLS observes UTH.

From the GCI the fractional coverage by cold cloud, η_c, is defined from individual 0.5° pixels, averaged over an area 4° × 4°, by clouds colder than a specified threshold. η_c measures the horizontal coverage by deep convection that invades the upper troposphere.

Supporting satellite observations of cloud and UTH are temperature and other meteorological fields in reanalyses from the European Centre for Medium-Range Weather Forecasts. They span the troposphere and are available four-times daily, compared to daily for mapped distributions of UTH and eight-times daily for the GCI.

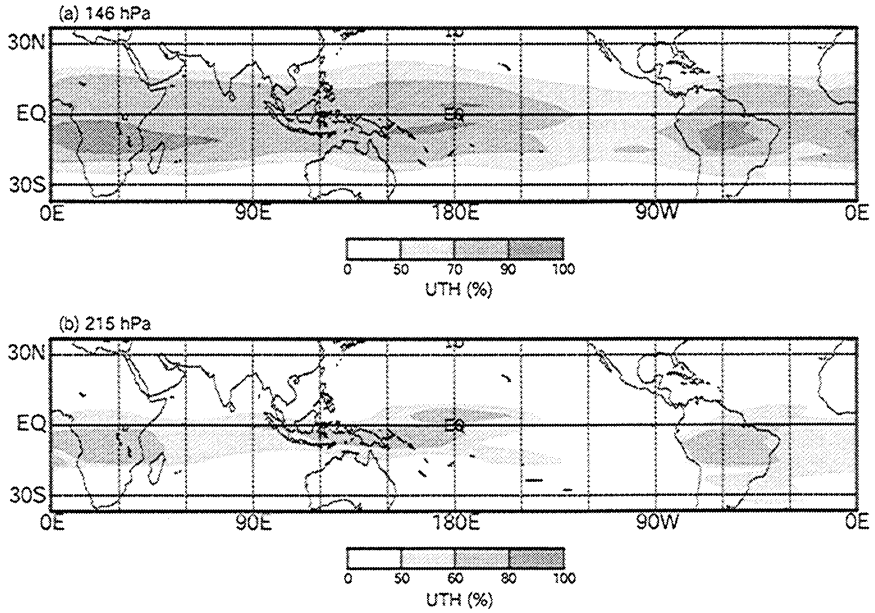

Figure 1. Time-mean distribution of UTH for January 1992 at (a) 146 hPa and (b) 215 hPa.

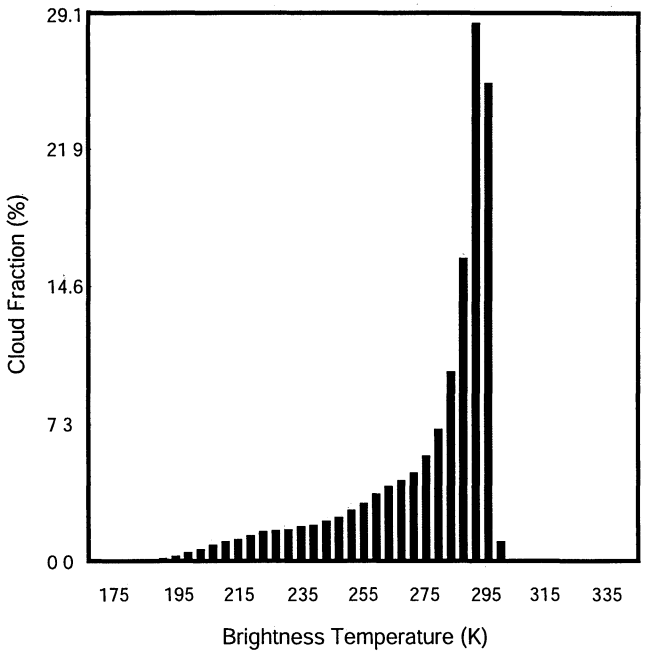

Figure 2. Cloud fraction η over the western Pacific, during February 1989, as a function of brightness temperature.

3. Three Dimensional Structure of Moisture and Cloud

3.1. Horizontal Structure. Time-mean distributions of UTH for January 1992 are shown in Figure 1 at 146 hPa and 215 hPa. UTH increases upward, reflecting the decrease with height of tropospheric temperature that brings air closer to saturation. At 146 hPa (Figure 1a), where temperature and saturation mixing ratios are lowest, UTH is enhanced over much of the tropics. The extensive structure of high humidity at this level is visible even in daily synoptic maps of UTH (Section 4). Over Africa, the central Pacific, and South America, air is close to saturation. As these conditions appear in the time-mean distribution, it follows that air over those regions is maintained close to saturation during most of the period averaged. At 215 hPa (Figure 1b), air is farther from saturation. The area occupied by almost saturated air is also less extensive than UTH at 146 hPa. Maximum humidity is now concentrated more over Africa, the central Pacific, and South America. At 315 hPa (not shown), enhanced UTH is concentrated about those regions even more.

Regions of enhanced UTH are also regions of deep convection, which is marked by cold cloud. Figure 2 presents a histogram of fractional cloud cover, η, in the tropics, as a function of brightness temperature T. η decreases sharply with T, cloud reaching the upper troposphere ($T \leq 235$ K) having fractional coverage of only a few percent. Coldest cloud, that with $T \leq 210$ K, has only about half the coverage of warmer cloud with $T \leq 235$ K. Notice that the histogram of η levels off at temperatures of 240 K – 210 K. Reflecting increased coverage relative to that anticipated from lower levels, this feature of cloud statistics represents cloud detrainment and the formation of extensive cirrus anvil that prevail at these levels of the upper troposphere.

Figure 3 shows time-averaged distributions of cold-cloud fraction, η_c, for the same period as in Figure 1. η_c represents brightness temperatures colder than 210 K and 230 K, which correspond to cloud at approximately

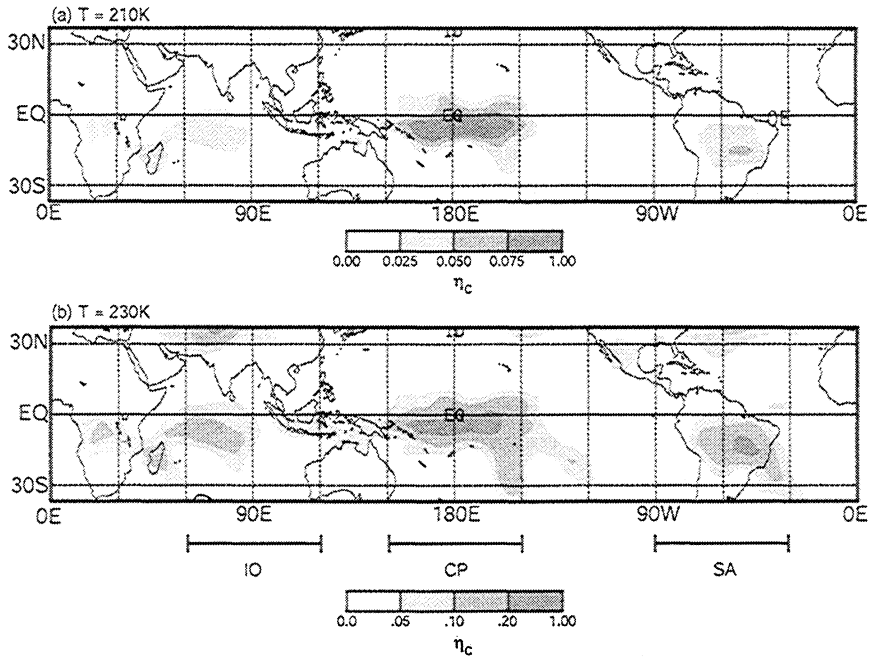

Figure 3. Cold cloud fraction η_c, averaged over January 1992. The η_c is calculated for brightness temperatures (a) colder than 210 K and (b) colder than 230 K. Note that different shading levels are used in the two panels. Indicated at bottom are longitudinal sectors over the Indian Ocean (IO), Central Pacific (CP), and South America (SA).

the same altitudes as UTH in Figure 1. Cloud colder than 210 K (Figure 3a) is concentrated over the central Pacific (CP), over Africa and the Indian Ocean (IO), and over South America (SA). Cold cloud is largely absent from the western Pacific during this period, when warm sea surface temperature (SST), supported by the Madden-Julian oscillation (MJO), has shifted convection eastward to the dateline [*Sandor et al.*, 1998]; see *Madden and Julian* [1994] for a review. Warmer cloud, with $T \leq 230$ K (Figure 3b), extends over more of the tropics. However, the largest η_c is still found in the central Pacific, with secondary maxima that mirror colder cloud in Figure 3a over Africa, the Indian Ocean, and South America.

The correspondence between time-mean distributions of UTH and cold-cloud fraction is strong: Locations of enhanced UTH are also locations of large η_c [see also *Read et al.*, 1995], although horizontal transport also influences UTH structure (section 4). A similar correspondence appears in column-averaged UTH representative of a much deeper layer above 500 hPa [*Soden and Fu*, 1995]. Although coldest cloud reaching 146 hPa ($T \leq 210$ K) is less prevalent than warmer cloud reaching 215 hPa ($T \leq 235$ K), high humidity over much of the layer centered at 146 hPa indicates that convection still contributes importantly to UTH near the tropopause.

Structural differences between UTH at 146 hPa and lower levels are noteworthy. At 146 hPa, UTH is fairly continuous and extends over much of the tropics. This structure contrasts with the more localized nature of η_c in Figure 3, which is concentrated in centers of convection. The extensive structure of UTH at upper levels is apparent even in daily synoptic maps, in which moist air streams out of convective centers (section 4). It is consistent with the cloud fraction histogram (Figure 2) leveling off at altitudes where extensive anvil forms. On the other hand, UTH at lower levels becomes concentrated about convective centers, mirroring the distribution of cold cloud. The change of character indicates that near the tropical tropopause the distribution of UTH comes increasingly under the influence of horizontal transport. Outflow from convective centers assumes the form of poleward and zonal motion that comprise horizontal branches of the Hadley and Walker circulations, respectively. Conversely, UTH at lower levels is controlled more by vertical transport, associated with upward motion inside convection that comprises ascending branches of those circulations.

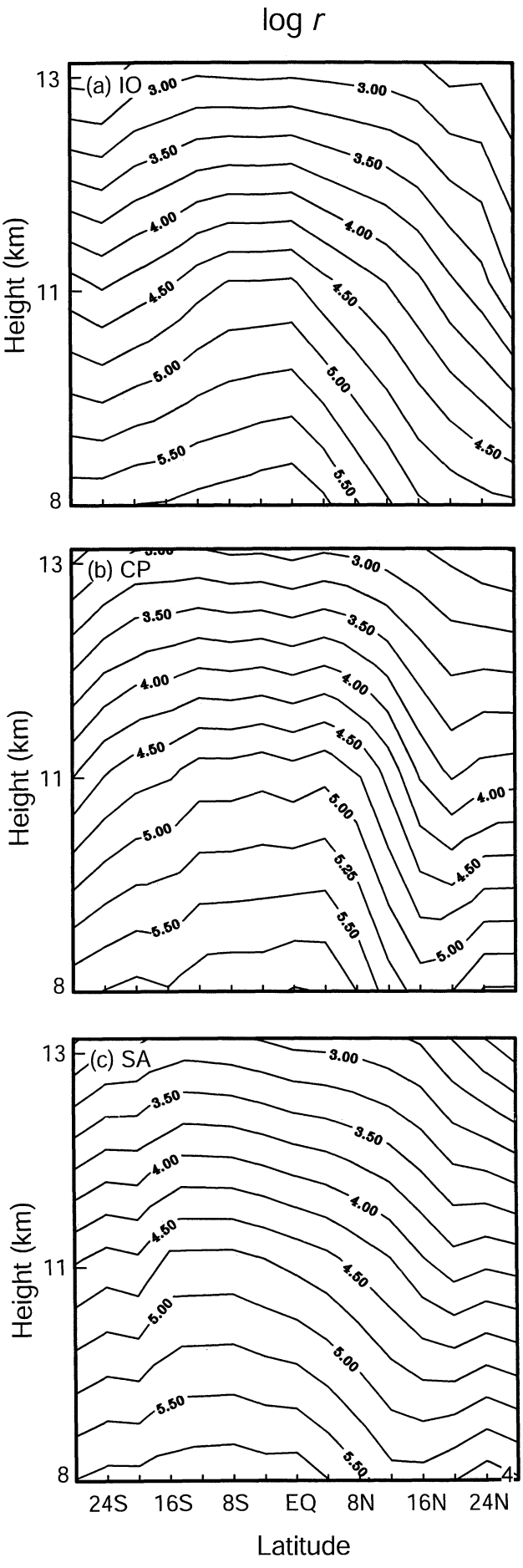

Figure 4. Logarithm of time-mean volume mixing ratio, as a function of latitude and altitude, for January 1992 based on analyzed temperature from the European Centre for Medium-Range Weather Forecasts (ECMWF); averaged zonally over (a) Indian Ocean, (b) Central Pacific, and (c) South America (see Figure 3). Contour interval is 0.25.

3.2. Vertical Structure

Zonal sectors where the correspondence between η_c and moisture is strong are indicated at the bottom of Figure 3. For each we calculate the volume mixing ratio r, averaged over longitude. Figure 4 plots log r (natural logarithm of mixing ratio in parts per million), as a function of latitude and height, for the three sectors of enhanced η_c and UTH. From the middle troposphere, r decreases upward sharply in each sector. Largest mixing ratios are found at the lowest level plotted, just south of the equator. This coincides with the region in which deep convection is concentrated. Also apparent at lower levels is the concentration of enhanced UTH about convective centers (e.g., over the central Pacific between 16°S and 8°N), which gives way at upper levels to broader enhancement. (Note that the logarithmic contour scale in Figure 4 deemphasizes horizontal variations. When UTH is displayed linearly, enhanced moisture at lower levels is concentrated even more at latitudes of convection.)

Structure in the northern (winter) subtropics is noteworthy. Over the Indian Ocean (Figure 4a), r decreases northward monotonically. This contrasts with structure over the central Pacific and South America (Figure 4b and 4c), where r first decreases and then actually increases northward. Separating these latitudes is a region in which mixing ratio surfaces are sharply depressed. The depression of r surfaces in the winter subtropics contrasts with their elevation in the tropics, inside regions of cold cloud.

Sectors in which the depression of mixing ratio surfaces is pronounced are the same ones in which convection is strong and cold-cloud fraction is large. Over each, a sharp minimum in r is found at 10°N - 20°N, where isopleths of r are deflected downward. Those latitudes are virtually cloud free (cf. Figure 3). r is therefore conserved, so it behaves as a tracer of air motion. The depression of mixing ratio surfaces thus reflects downwelling over the subtropics of the winter hemisphere. It corresponds to the descending branch of the Hadley circulation, which transports downward drier air from aloft and is strong in the winter hemisphere. Found along the northern flank of convective centers, this local vertical structure is consistent with horizontal changes operating on seasonal timescales that have been reported in column-averaged UTH [*Soden and Fu*, 1995].

Further northward, isopleths of r become approximately horizontal. Isentropic mixing by baroclinic eddies acts to level mixing ratio surfaces at those latitudes, simultaneously exchanging moist tropical air with drier air from higher latitudes (see Figure 7a). Visible over a deep layer above 8 km, the leveling of r surfaces in Figure 4 involves much of the troposphere.

Figure 5 shows analogous information for cloud fraction, as a function of brightness temperature. In each zonal sector, η is large south of the equator (in the summer hemisphere), where contours are elevated, and it decreases northward (into the winter hemisphere), where contours are sharply depressed. Near 16°N, no cloud is observed, not even at the warmest T. This structure of η is consistent with the depression of mixing ratio surfaces and downwelling inside the descending branch of the Hadley circulation. In contrast, cold cloud occurs frequently just south of the equator. The coldest and highest cloud is found over the central Pacific, where the MJO has displaced convection during this period. This is also the zonal sector in which depressions of η and r are deepest and positioned farthest north.

4. Instantaneous Behavior

4.1. Synoptic Distributions

The association between enhanced UTH and cold cloud, apparent in time-mean distributions, is also evident in daily distributions that have been synoptically mapped from MLS. Figure 6 plots a Hovmoller diagram of UTH at 215 hPa (contoured), as a function of longitude and time, which has been constructed from daily synoptic maps. Like its January-mean distribution, UTH is concentrated over the Indian ocean, the central Pacific, and over South America. However, it varies greatly from one day to the next, reflecting sporadic outbreaks of convection introduced by changes of the large-scale circulation.

Very similar behavior is exhibited by the fractional coverage of cloud colder than 230 K. Like UTH, η_c is concentrated over the Indian Ocean, the central Pacific, and South America, but varies greatly from one day to the next. Even though η_c and UTH are each noisy, sporadic amplifications of one are mirrored in the other, especially over South America, where convection operates diurnally. Reflected in both properties is a gradual eastward drift from the Indian Ocean to across the dateline (e.g., during days 10–40 and repeated during days 40–70, and again during days 80–100), when convection is modulated by the MJO. Also included are faster changes associated with synoptic disturbances and easterly waves (e.g., over South America). On all of these timescales, sporadic outbreaks of cold cloud are attended by enhancements of UTH.

Water vapor that has been conveyed to the upper troposphere is transported horizontally. Figure 7a shows the synoptic global cloud image at 2100 UT on December 29, 1991. Cold cloud appears over Africa, the Indian Ocean, the central Pacific, and South America. The contemporaneous map of UTH at 215 hPa, shown in Figure 7b, reveals high humidity in each convective center. Moist air streams away from these source regions: At latitudes of the coldest (brightest) cloud, humidified air has coalesced into a nearly continuous strip that extends across much of the Eastern Hemisphere. Simultaneously, moist air streams into the Northern

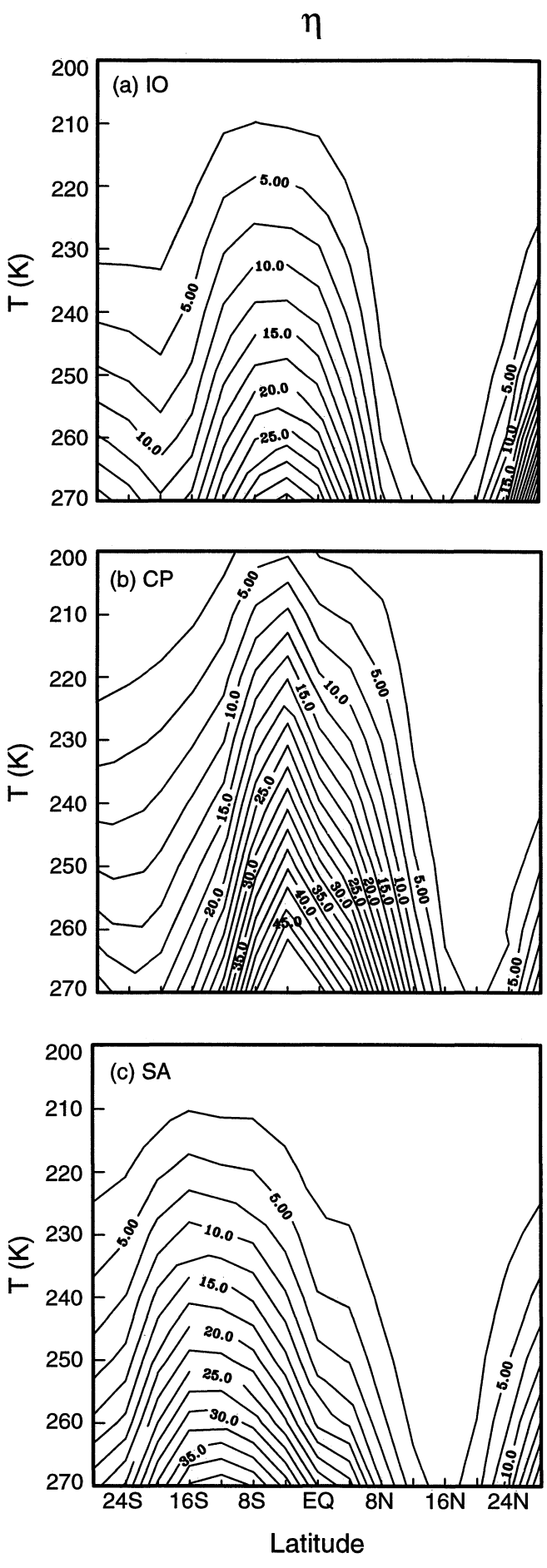

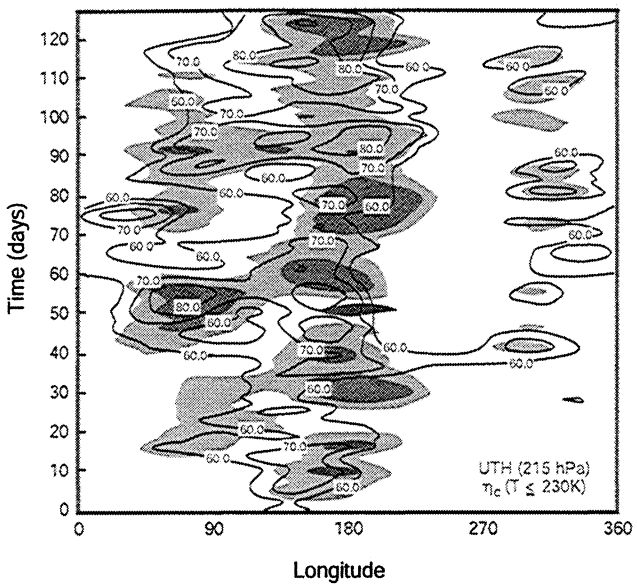

Figure 6. Hovmoller diagram of 215 hPa UTH (contoured), as a function of longitude and time, from November 4, 1991. Superposed is fractional coverage by cloud colder than 230 K η_c (shaded). Contour interval for UTH is 10% starting at 60%. Shading levels are 5% and 10%.

Hemisphere from the dateline, northeastward across the Pacific. It continues beyond the Caribbean over the Atlantic, eventually appearing over Europe on subsequent days. Analogous structure extends into the Southern Hemisphere (to the highest latitude observed by UARS during this month), where it joins the frontal system of a midlatitude cyclone (Figure 7a). Similar behavior is observed in the column abundance of water, which is concentrated at lower levels [*Randel et al.*, 1996]. For both advective features in Figure 7b, moist air avoids the tropical eastern Pacific, where descending motion of the Walker circulation depresses mixing ratio surfaces and maintains the upper troposphere cloud free.

Horizontal transport evident in Figure 7 enables convection to influence UTH remotely. Moist air introduced over one convective center is carried elsewhere, leading to variations of UTH other than those coupled locally to convection. Such behavior is evident in Figure 6 and is documented also in isentropic back trajectories of upper tropospheric parcels [*McCormack et al.*, 2000]. Transport by baroclinic systems at midlatitudes also acts to mix air horizontally, leveling mixing ratio surfaces as they drive thermal structure toward barotropic stratification. Several systems are visible in Figure 7a

Figure 5. Time-mean cloud fraction, as a function of latitude and brightness temperature, for January 1992; averaged over (a) Indian Ocean, (b) Central Pacific, and (c) South America. Contour interval is 2.5%.

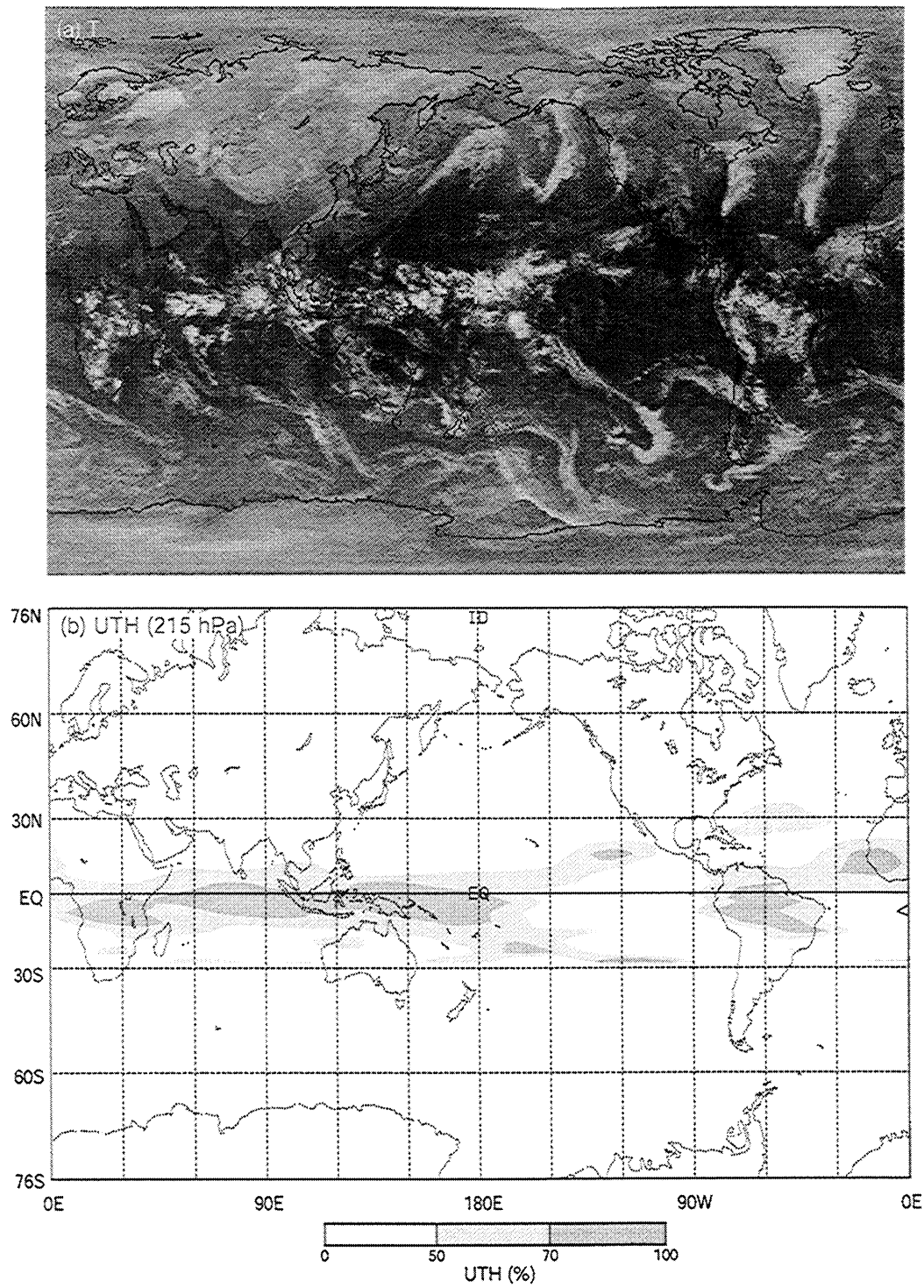

Figure 7. (a) Synoptic global cloud image at 2100 UT on December 29, 1991. (b) UTH on December 29, 1991, at 215 hPa. Shading levels are 50% and 70%

north of the convective center over the Pacific. They operate just beyond the neighboring clear-sky region, where r surfaces in Figure 4 have been leveled.

4.2. Spatial Coherence

UTH and η_c are strongly related in averages over a month, as well as in daily synoptic maps. For each, the implied relationship appears broad, cold cloud and moist air spanning large areas of the tropics. However, actual convective systems that underlie time-mean and daily distributions (e.g., Figure 7a) involve much smaller spatial dimensions and are intermittent. Those space and timescales are too short to be represented properly in asynoptic measurements of UTH. They can, however, be characterized statistically.

The autocorrelation function of r, c_r, has been calculated at high spatial resolution from nearly simultaneous measurements along ascending and descending

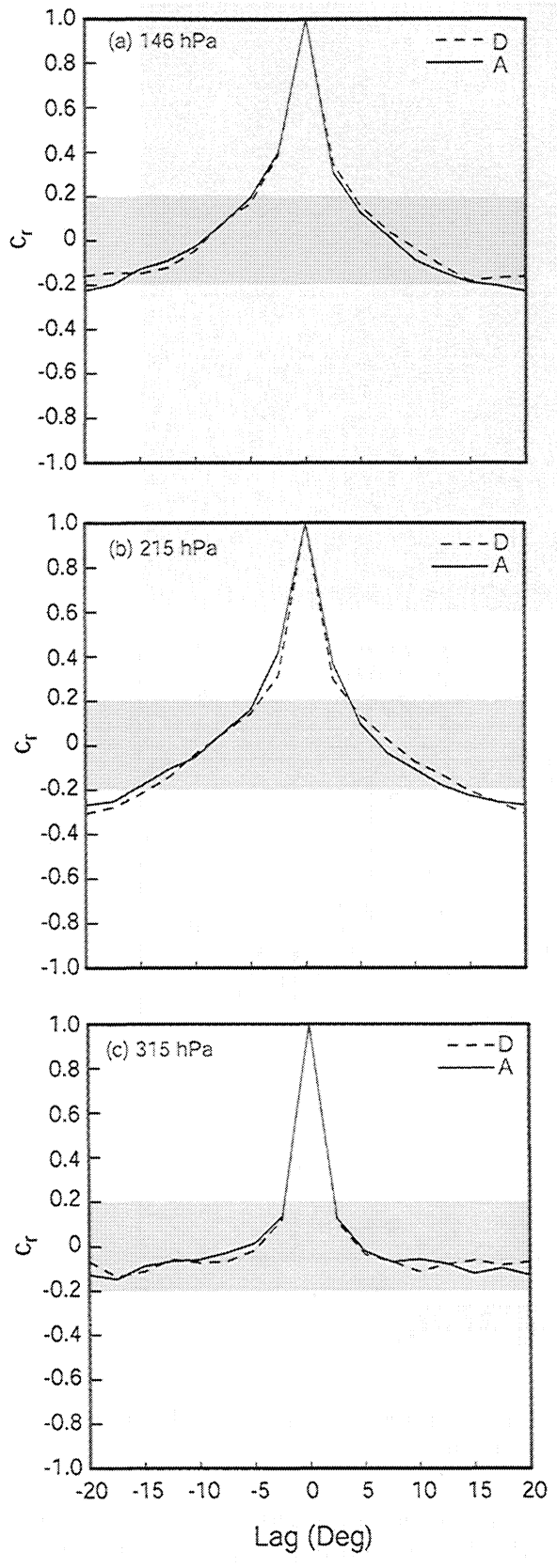

Figure 8. Autocorrelation function c_r of volume mixing ratio at (a) 146 hPa, (b) 215 hPa, and (c) 315 hPa. The 99% confidence interval is shaded. A and D indicate ascending and descending segments of the satellite orbit, respectively.

tracks of MLS. The c_r is calculated for individual tracks crossing the tropics over the central Pacific and then averaged over all tracks collected between October 2, 1991 and March 29, 1992. This statistical procedure represents fluctuations with resolution that is sufficiently fine to capture the structure of actual convective systems. A similar procedure is applied to cold-cloud fraction, which has been sampled in the GCI at the same space-time coordinates as MLS observes UTH. (As convection in the GCI is statistically isotropic, the correlation function obtained along satellite tracks provides a good representation of horizontal coherence along any direction.)

Figure 8 plots c_r as a function of horizontal lag. At each level, c_r is sharply peaked at zero lag. At 146 hPa and 215 hPa (Figures 8a and 8b) it falls below the the 99% confidence level (shaded field) beyond a lag of only 5°. The c_r at 315 hPa (Figure 8c) is similar. However, it is peaked even more narrowly, falling below 99% confidence beyond a lag of only 2.5°. The shorter correlation scale reflects smaller instantaneous structure. It mirrors the change in time-mean structure (section 3) that in analogous fashion, becomes concentrated about convective centers at lower levels.

The correlation scale of UTH, which characterizes its instantaneous structure, is comparable to the horizontal dimension of the region scanned by MLS, which observes UTH through the limb of the atmosphere. Consequently, MLS observations of UTH at adjacent latitudes along the orbital track (separated by ~3°) are nearly independent. More importantly, the narrow correlation scale suggests that, ultimately, it is limited by the viewing geometry and separation of MLS measurements. Actual anomalies of UTH may be even narrower, especially at lower levels.

For comparison, Figure 9 shows the autocorrelation function of cold-cloud fraction c_{η_c}, for brightness temperatures representative of the levels at which UTH is shown in Figure 8. The c_{η_c} resembles c_r. It, too, is sharply peaked at zero lag, falling below 99% confidence beyond a lag of only 2.5°. That is comparable to the correlation scale of UTH at the lowest level shown in Figure 8, where vertical transport concentrates humidity about convective centers. Unlike UTH, however, the correlation function of η_c exhibits no systematic change with height; it retains the same narrow scale at all levels. UTH, on the other hand, becomes broader at 215 and 146 hPa, reflecting the increased role of horizontal transport on water vapor that has been carried to those levels.

5. Convective Influence on Thermal Structure

Further support for the relationship of UTH to deep convection comes from thermal structure in the upper troposphere. Figure 10 shows vertical sections of time-mean potential temperature (θ) during January 1992

along the dateline and at 90°W. These locations are characteristic of deep convection and no convection, respectively (cf. Fig. 3). In the central Pacific (Figure 10a) the vertical separation of θ surfaces is expanded inside a deep layer centered at ~200 hPa. There, the 350 K isentropic surface is displaced upward relative to its position under nonconvective conditions (Figure 10b). Simultaneously, the 340 K isentropic surface is displaced downward. Vertical stability is thus reduced inside the region of convection, where vertical mixing acts to homogenize θ and drive buoyancy (N^2) toward zero.

The expansion of θ surfaces is most pronounced in the upper troposphere, maximizing around 200 hPa. This is the same region where the histogram of cloud fraction (Figure 2) levels off, reflecting cloud detrainment and the formation of extensive anvil. The expansion of θ surfaces decreases at higher levels, vanishing near θ = 375 K, above which the close spacing of θ surfaces and large N^2 characterize stratospheric air.

The impact of convective mixing is also manifested in the horizontal distribution of θ. Figure 11 plots θ at levels for which UTH and η_c were considered earlier. At 146 hPa (Figure 11a), θ possesses a broad minimum near the equator. Smallest θ appears over Africa, the Indian Ocean, the central Pacific, and South America. In fact, locations in Figure 11a where $\theta \leq 351$ K (bold) resemble those where η_c and UTH are enhanced (Figure 1a and 3a). At 215 hPa (Figure 11b), θ possesses a maximum in the tropics, reflecting the reversal in slope of isentropic surfaces at and beneath 11 km (Fig. 10). The convective center over the central Pacific is well defined at this level, where vertical transport prevails, mirroring structure of r and η_c (Figure 1b and 3b). Centers over Africa and South America are also visible, corresponding to analogous features in r and η_c. Similar structure punctuates the distribution of θ at 315 hPa (Figure 11c).

6. Statistical Description of Moisture and Cloud

Air mixed vertically by convection ventilates the upper troposphere, conveying moisture from its reservoir at the surface. This process serves as a source of UTH, which is enhanced in regions of cold cloud. It humidifies isentropic layers, in which water vapor is subsequently advected by the large-scale circulation.

In reality, UTH is forced on the scales of individual convective systems. They are too small to be resolved in asynoptic measurements. However, their collective impact on daily and time-mean distributions can be evaluated statistically.

6.1. Joint Occurrence of Enhanced Moisture and Cold Cloud

The relationship between convection and moisture is expressed by the joint probability density function (pdf)

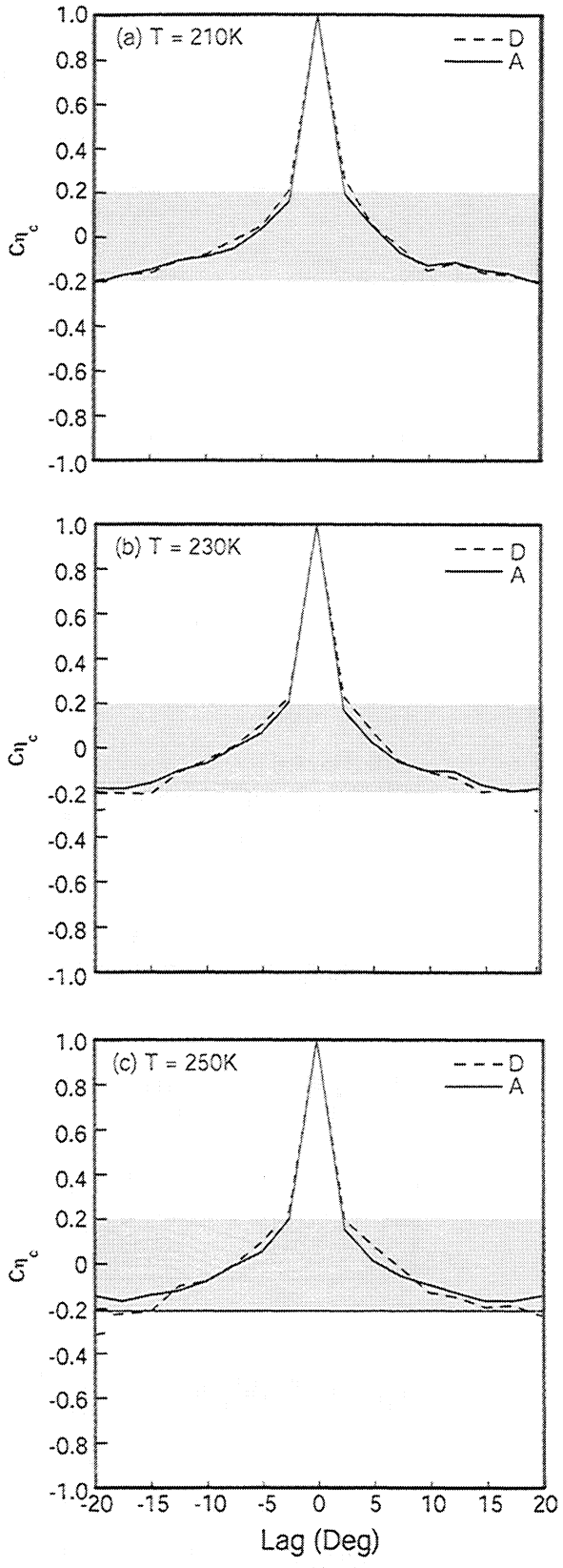

Figure 9. Autocorrelation function c_{η_c} of cold clo9d fraction for brightness temperatures colder than (a) 210 K, (b) 230 K, and (c) 250 K. The 99% confidence interval is shaded.

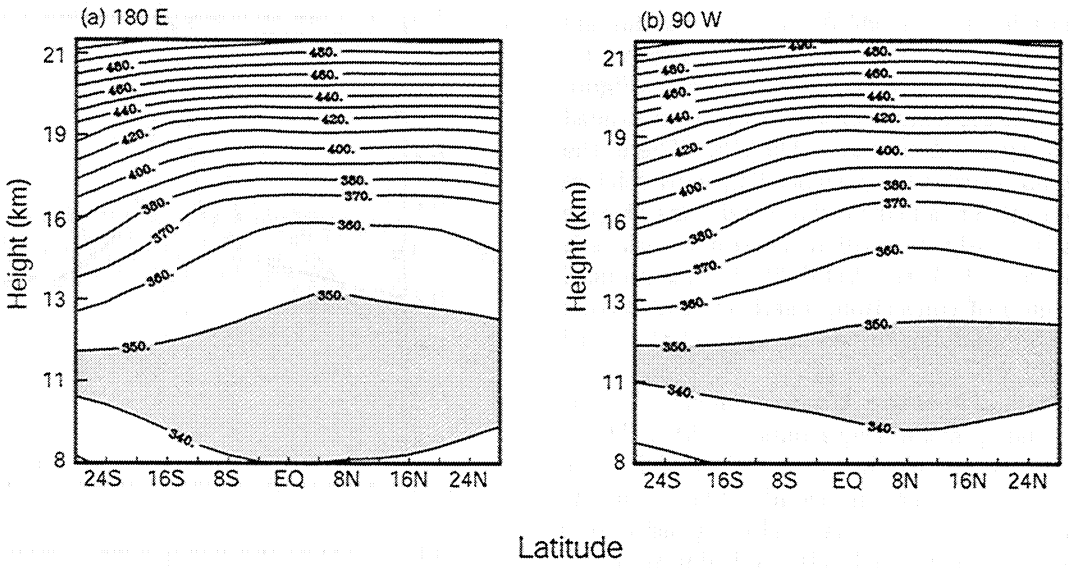

Figure 10. Potential temperature, as a function of latitude and altitude, for January 1992 at (a) 180°E and (b) 90°W. Contour interval is 10 K.

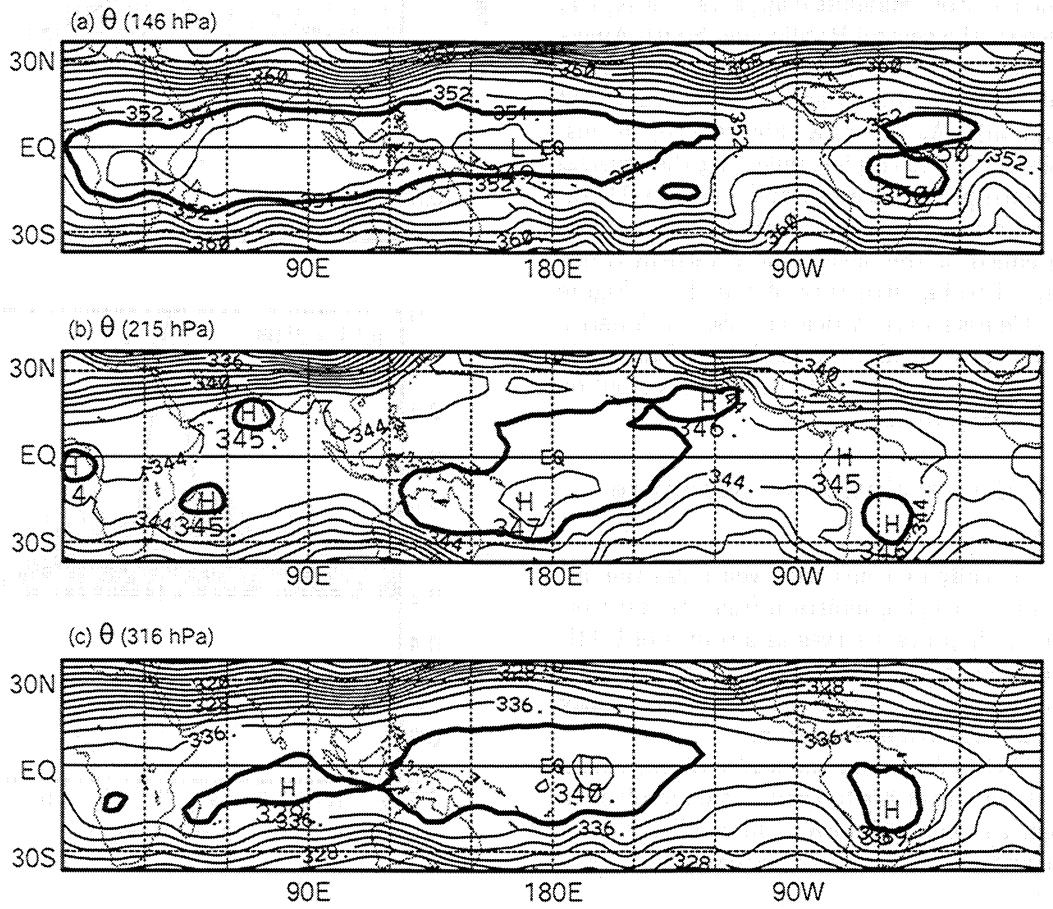

Figure 11. Time-mean distributions of potential temperature for January 1992, at (a) 146 hPa, (b) 215 hPa, and (c) 316 hPa. Contour interval is 2 K in Figure 11a, 1 K in Figure 11b, and 2 K in Figure 11c. Bold contours indicate θ =351 K in Figure 11a, θ =345 K in Figure 11b, and θ =338 K in Figure 11c.

of moist air and cold cloud: It measures the probability of simultaneous observations of cold cloud in the interval $(\eta,\eta + d\eta)$ jointly with upper tropospheric humidity in the interval (UTH,UTH+dUTH). The joint pdf relates humidification of the upper troposphere to cold-cloud fraction. Attention focuses now on the isentropic layer centered at 215 hPa that is bounded by the surfaces θ=340 K and 350 K (see Figure 10). This layer characterizes the region where θ surfaces are most expanded. Enhanced moisture is defined as MLS observations exceeding the threshold UTH $\geq$ 70%. During the period October 2, 1991 – April 28, 1992, measurements of UTH satisfying this criterion define a population of enhanced moisture observations. Corresponding sites of space and time are then sampled asynoptically in the GCI for cold cloud that invades the region above θ = 340 K. The associated cloud fraction η_c measures convective cloud that ventilates the isentropic layer under consideration.

Figure 12 shows, as a function of η_c, the pdf of enhanced moisture that is observed coincidentally with cold cloud: that is the integral of the joint pdf for UTH $\geq$70%. Over the Indian Ocean (Figure 12a) the pdf of enhanced moisture is broad, maximizing at small cloud fraction. Over the central Pacific (Figure 12b) the pdf is almost uniform over all bins of cloud fraction. Over South America (Fig. 12c), the pdf peaks at small η_c and decreases monotonically. The pdf in this region is also distinguished by a significant difference between ascending and descending data, reflecting the strong diurnal cycle of convection present over land (Diurnal variations in r and η_c recovered by MLS sampling are weakened by the precessing orbit of UARS, which drifts through local time. Over the period under consideration, MLS observations have cycled completely through 24 hours of local time nearly three times.)

The joint pdf in Figure 12 describes opportunities for water vapor to reach the upper troposphere, ventilating the isentropic layer under consideration. The pdf differs between land and sea. Over maritime regions of warm SST, convection taps the reservoir of surface moisture. Enhanced UTH is then largely independent of η_c: It occurs with comparable frequency in all ranges of cloud fraction. Conversely, over continental regions, convection relies instead on the strong diurnal variation of surface temperature. Enhanced UTH is then found preferentially with cloud that appears at this level most frequently (Figure 2), that with small η_c. As that range of cloud fraction also occurs at a preferred local time, UTH over continental regions should vary diurnally.

The joint pdf determines the expected value of mixing ratio, $\langle r \rangle$: that value of r most likely to be observed for a given η_c. It equals the mean value of r in the population of measurements for a specified range of cloud fraction. The $\langle r \rangle$ characterizes large-scale or net humidification of the isentropic layer by deep convective cloud. By collecting the overall influence from a population of convective features it describes the process underlying

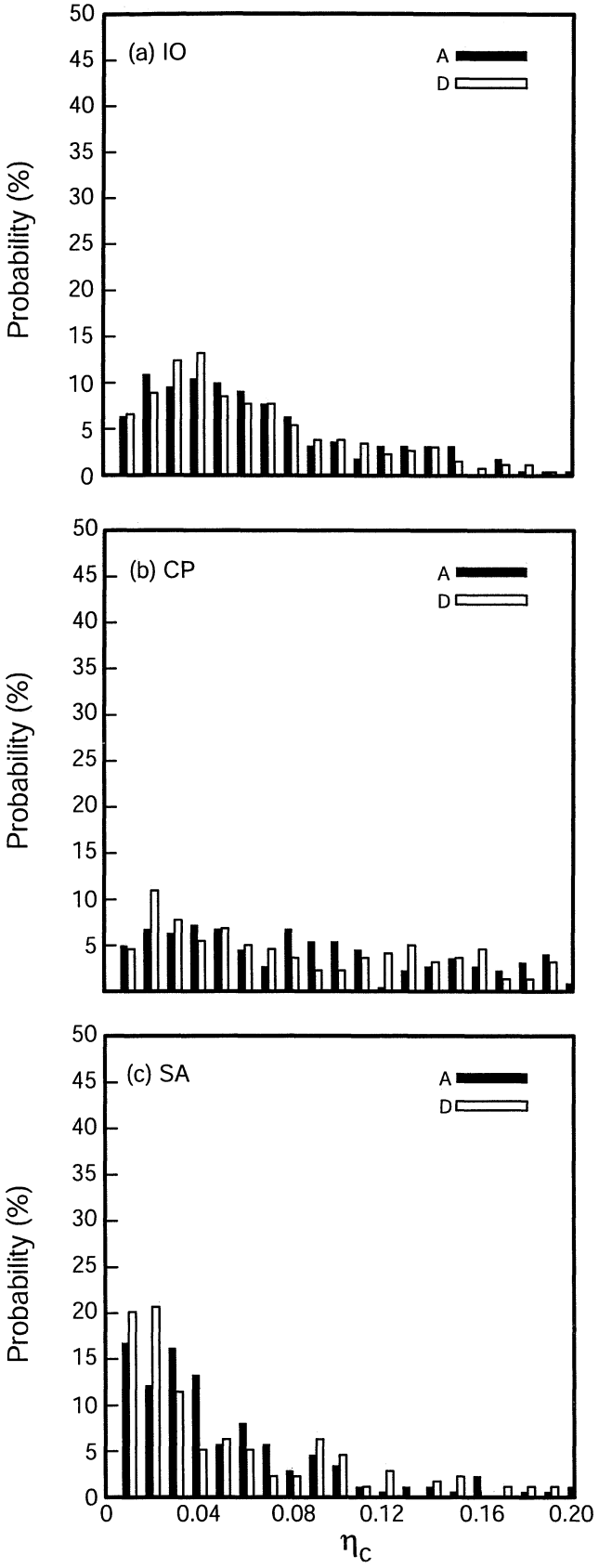

Figure 12. Joint probability density function of moist (UTH > 70%) and cold cloud ventilating the isentr11ic layer above 340 K, over (a) Indian Ocean, (b) Central Pacific, and (c) South America. Black (white) bars correspond to ascending (descending) tracks of the orbit.

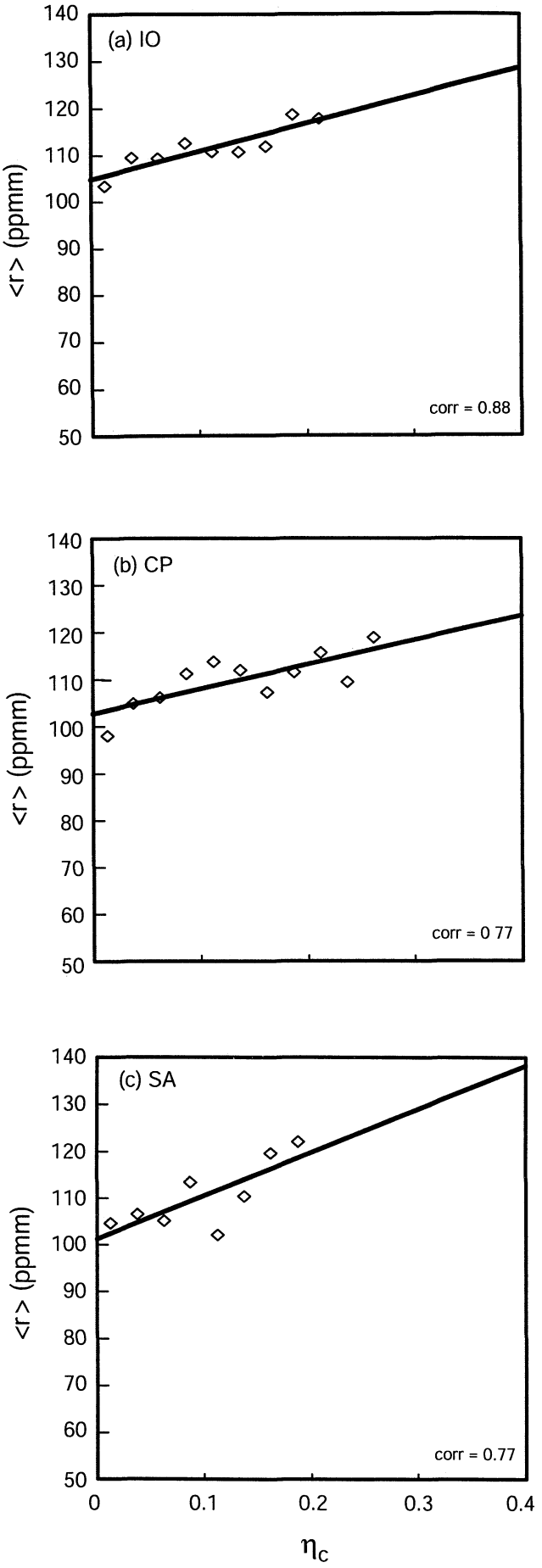

coherent variations of UTH, like those represented in daily and time-mean distributions.

Expected values are plotted in Figure 13, as a function of η_c, over the three zonal sectors. Over each, $\langle r \rangle$ exhibits a positive, indeed, almost linear relationship to η_c: Increased cold-cloud fraction is attended by enhanced UTH inside the isentropic layer. Correlations between $\langle r \rangle$ and η_c in the three convective centers range from 0.77 to as high as 0.88. These are comparable to correlations for column-averaged UTH over a much deeper layer *Soden and Fu*, 1995. Significant at the 99 – 99.9% level, they imply that some 60–80% of the coherent UTH variance is accounted for by variations of convective cloud that ventilates the isentropic layer.

6.2. Relationship Between Moist and Dry Regions

Enhancement of UTH by convection expands the horizontal extent of the optically thick region of moist air, while contracting the optically thin region of dry air. At the same time, UTH is reduced inside sinking air that has recently been desiccated by condensation. The latter process is clearly visible poleward and eastward of convective centers (Figures 4 and 7), where the depression of mixing ratio surfaces reflects descending branches of the Hadley and Walker circulations, respectively. It is of interest to determine the relationship between moist and dry regions, in particular, how one changes in response to a change in the other. We consider this in the fractional coverage by moist and dry regions.

Figure 14 plots the fractional coverage over the tropics by moist air at 215 hPa having UTH≥70% (solid). It is compared against the fractional coverage by dry air having UTH≤40% (dashed line). The two areas exhibit compensating changes, having a correlation of –0.67. When moist air expands, during outbreaks of deep convection, dry air recedes and vice versa. The net change of tropical UTH thus follows as a small residual of these two offsetting changes.

Superposed in Figure 14 is the record of UTH averaged over the tropics as a whole (dotted line). It is strongly correlated to the fractional coverage by moist air, having a correlation of 0.72. Increased coverage by moist air thus leads to increased UTH over the tropics as a whole. From the strong relationship between UTH and cold-cloud fraction it follows that the collective effect of deep convection is to humidify the upper troposphere. Increased deep convection leads to enhanced UTH over the tropics.

Figure 13. Expected value of r (diamond) in mass mixing ratio, obtained from the probability density function of descending orbital tracks in Figure 12 for (a) Indian Ocean, (b) Central Pacific, and (c) South America. Bold line represents linear regression of expected values. Correlation coefficient is shown at the bottom.

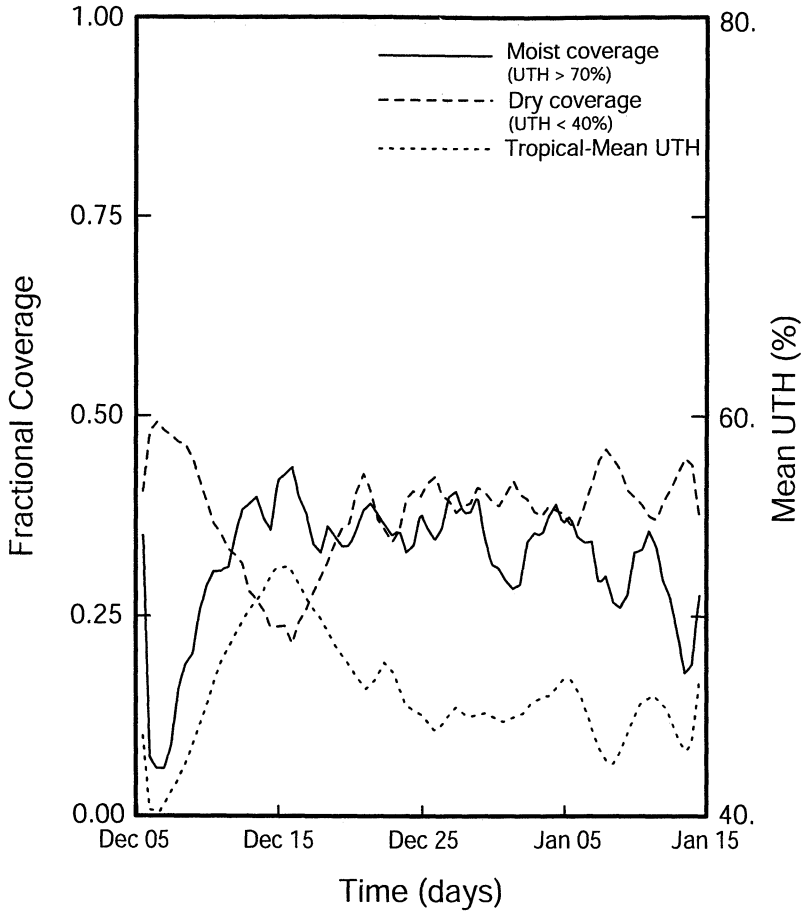

Figure 14. Fractional coverage over the tropics by moist air (solid line) and dry air (dashed line), as a function of time. Superposed is tropical-mean UTH (dotted line).

This finding, which applies to shallow layers at and beneath the tropopause, echoes a similar conclusion drawn from column-averaged UTH representative of a much deeper layer [*Soden and Fu*, 1995]. It characterizes forcing of UTH in the global moisture budget. The same process affects global energetics by controlling the area covered by moist and dry air, which contributes disproportionately to outgoing longwave (LW) flux. Outgoing longwave radiation (OLR) depends quartically on brightness temperature, which in turn depends on humidity. In dry areas, which are optically thin, LW radiation is emitted from lower levels that are warmer. Consequently, dry areas contribute much more to OLR, per unit area, than do moist areas that are optically thick. An increase of UTH over the tropics, introduced by an increase of convection, would then increase greenhouse warming. However, the net change of OLR could actually follow principally from the contraction of dry optically thin areas, closing the holes through which much of the radiation passes.

7. Conclusions

The striking correspondence between UTH and cold cloud, in time-mean distributions, in synoptic maps, and even in instantaneous structure that characterizes individual convective systems, implies that moisture in the tropical upper troposphere is forced by deep convection. At lower levels, UTH observed by MLS is concentrated about centers of cold cloud, reflecting the dominant role of vertical transport in supplying those levels with moisture from below. However, at levels neighboring the tropopause, high humidity extends continuously over much of the tropics. The change of structure is analogous to behavior in the histogram of cloud fraction, which reflects cloud detrainment at these levels and the formation of cirrus anvil. It corresponds to UTH coming increasingly under the control of horizontal transport, as air convected to the upper troposphere attains its lowest temperature and saturation mixing ratio, diverges, and mixes with its surroundings inside extensive anvil. It is noteworthy that this change of structure is not resolved in conventional measurements with inferior vertical resolution, wherein layers of different structure are averaged together.

Flanking regions of cold cloud and enhanced UTH are regions in which the upper troposphere remains cold free and dry. The depression of mixing ratio surfaces, notably in the winter subtropics and eastern Pacific, reveals descending motion of the Hadley and Walker cir-

culations, which transport down drier air. The meridional overturning is zonally asymmetric, mirroring the structure of deep convection. It is strongest in the winter subtropics at those longitudes where convection is strongest and deepest. Poleward extent of the meridional overturning is limited by horizontal mixing by midlatitude baroclinic systems, which level r surfaces as they drive thermal structure toward barotropic stratification. This zonally asymmetric picture of moisture is consistent with the poleward extent of the Hadley circulation being limited by baroclinic instability at midlatitudes *Gill*, 1982.

Ventilation of the upper troposphere is also evidenced by thermal structure, which contrasts between convective and nonconvective regions. Convective mixing leads to reduced vertical stability in regions where cold-cloud fraction and UTH are high. This causes θ surfaces in the uppermost troposphere to dome upward, analogous to mixing ratio surfaces. The signature of convective mixing maximizes in a deep layer centered at ~200 hPa, where stability is reduced most. This coincides with the layer of extensive anvil, where air diverges away from convective centers and the UTH distribution becomes horizontally extensive.

Deep convection serves as a source of water vapor in the global moisture budget. UTH over the tropics as a whole increases almost linearly with cold-cloud fraction. This follows from humidification, which expands the area covered by moist air, and desiccation, which contracts the area covered by dry air. As most of the optical depth at these levels follows from water vapor, the relationship to cold cloud implies increased greenhouse trapping of LW radiation under conditions of increased deep convection. From the standpoint of the global energy budget, however, moist and dry areas are not equally weighted. OLR emanating from each depends nonlinearly on brightness temperature, which in turn depends on humidity. Since dry areas contribute disproportionately to OLR, the contraction of those optically thin areas under conditions of increased convection may dominate the net change of OLR. The net change also depends on the area covered by cold cloud, which is also optically thick and, as seen here, is strongly correlated to UTH.

Acknowledgments. The authors thank J. Waters for comments provided on this manuscript. This work was supported by NASA grants NAG5-6692 and NAG5-4666.

References

Gill, A.E., *Atmosphere-Ocean Dynamics.* 662 pp., Academic, San Diego, Calif., 1982.

Madden, R. A. , and P. R. Julian, Observations of the 40-50 day tropical oscillation: A review, *Mon. Weather Rev.*, *122*, 814-837, 1994.

McCormack, J.P., R. Fu, and W.G. Read, The influence of convective outflow on water vapor mixing ratios in the tropical upper troposphere: An analysis based on UARS MLS measurements, *Geophys. Res. Lett.*, *27*, 525-528, 2000.

Randel, D.L., T.H Vonder Haar, M.A. Ringerud, G.L. Stephens, T.J. Greenwald, and C.L. Combs, A new global water vapor dataset, *Bull. Amer. Meteorol. Soc.*, *77*, 1233-1246, 1996.

Read, W. G., J. Waters, D.A. Flower, L. Froidevaux, R.F. Jarnot, D.L. Hartmann, R.S. Harwood, and R.B. Rood, Upper tropospheric water vapor from UARS MLS, *Bull. Am. Meteorol. Soc.*, **76**, 2381-2389, 1995.

Riehl, H., and J.S. Malkus, On the heat balance of the equatorial trough zone, *Geophysica*, *6*, 503-537, 1958.

Salby, M. and F. Sassi, Synoptic mapping of convective structure in undersampled satellite observations, *J. Clim.*, in press, 2001.

Salby, M. L., H.H. Hendon, K. Woodberry, and K. Tanaka, Analysis of global cloud imagery from multiple satellites, *Bull. Am. Meteorol. Soc.*, *72*, 467-480, 1991.

Sandor, B.J., W.G. Read, J.W. Waters, and K.H. Rosenlof, Seasonal behavior of tropical to midlatitude upper tropospheric water vapor from UARS MLS, *J. Geophys. Res.*, *103*, 25,935–25,947, 1998.

Soden, B. J., and R. Fu, A satellite analysis of deep convection, upper-tropospheric humidity, and the greenhouse effect, *J. Clim.*, *8*, 2335-2351, 1995.

Tanaka, K.H., K. Woodberry, H.H. Hendon, and M.L. Salby, Assimilation of global cloud imagery from multiple satellites, *J. Atmos. Oceanic Tech.*, *8*, 613-626, 1991.

Waters, J. W., et al., The UARS and EOS Microwave Limb Sounder (MLS) experiments, *J. Atmos. Sci.*, *56*, 194-218, 1999.

Zhu, Y., R.E. Newell, and W.G. Read, Factors controlling upper tropospheric water vapor, *J. Clim.*, *13*, 836-848, 2000.

W. G. Read, Jet Propulsion Laboratory, California Institute of Technology, Mail Stop 183-701, 4800 Oak Grove Drive, Pasadena, CA 91109. (bill@mls.jpl.nasa.gov)

M. Salby, Program in Atmospheric and Oceanic Sciences, University of Colorado, 311 UCB, Boulder, CO 80309. (murry.salby@colorado.edu)

F. Sassi, Atmospheric Systems and Analysis, 1400 West 122nd Avenue. Suite 101, Westminster, CO 80234. (sassi@asac.org)

(Received September 13, 2000; revised January 17, 2001; accepted January 23, 2001.)